atmosphere

MDPI

Article

Feasibility Study of Rain Rate Monitoring from Polarimetric GNSS Propagation Parameters

Hao An, Wei Yan *, Yunxian Huang, Xianbin Zhao, Yingqiang Wang and Weihua Ai

College of Meteorology and Oceanography, PLA University of Science and Technology, Nanjing 211101, China; 13770997977@163.com (H.A.); 13813891802@163.com (Y.H.); xian854591504@126.com (X.Z.); wyqiang198253@163.com (Y.W.); awhzjax@126.com (W.A.)

* Correspondence: 18913979082@163.com; Tel.: +86-25-8083-0276

Academic Editor: Robert W. Talbot

Received: 15 October 2016; Accepted: 30 November 2016; Published: 6 December 2016

Abstract: In this work, the feasibility of estimating rain rate based on polarimetric Global Navigation Satellite Systems (GNSS) signals is explored in theory. After analyzing the cause of polarimetric signals, three physical-mathematical relation models between co-polar phase shift (K_{HH}, K_{VV}), specific differential phase shift (K_{DP}), and rain rate (R) are respectively investigated. These relation models are simulated based on four different empirical equations of nonspherical raindrops and simulated Gamma raindrop size distribution. They are also respectively analyzed based on realistic Gamma raindrop size distribution and maximum diameter of raindrops under three different rain types: stratiform rain, cumuliform rain, and mixed clouds rain. The sensitivity of phase shift with respect to some main influencing factors, such as shape of raindrops, frequency, as well as elevation angle, is also discussed, respectively. The numerical results in this study show that the results by scattering algorithms T-matrix are consistent with those from Rayleigh Scattering Approximation. It reveals that they all have the possibility to estimate rain rate using the K_{HH}-R, K_{VV}-R or K_{DP}-R relation. It can also be found that the three models are all affected by shape of raindrops and frequency, while the elevation angle has no effect on K_{HH}-R. Finally, higher frequency L1 or B1 and lower elevation angle are recommended and microscopic characteristics of raindrops, such as shape and size distribution, are deemed to be important and required for further consideration in future experiments. Since phase shift is not affected by attenuation and not biased by ground clutter cancellers, this method has considerable potential in precipitation monitoring, which provides new opportunities for atmospheric research.

Keywords: rain rate; GNSS signals; co-polar phase shift; specific differential phase shift; T-matrix; sensitivity analysis

1. Introduction

The Global Navigation Satellite Systems (GNSS), mainly including the United States' Global Position System (GPS), Russia's GLONASS, China's BeiDou, and European Union's GALILEO, have been rapidly developed in the past few decades [1]. Along with its vigorous development of GNSS, the non-navigational applications of GNSS signals have attracted more and more attention, especially in the field of Atmosphere-Ocean and Space environmental remote sensing. Currently, some research has been put into operational systems, with some of these operational systems having been investigated by numerous experiments.

The zenith tropospheric delay (ZTD) along the GNSS signal path, which is one of the major error sources for GNSS positioning, can be used to detect precipitable water vapor (PWV) [2,3], and its three-dimensional distribution can be retrieved by ground-based GNSS station networks. The results of these research endeavors created a new science, GNSS meteorology. The GNSS Radio Occultation

(RO) signals received from mountain-based or space-based (Low-Earth-Orbit (LEO)) receivers are used to retrieve atmospheric temperature profiles, atmospheric moisture profiles, and total electron content (TEC) [4–6]. Using reflected signals of GNSS from different underlying surface, we can monitor the parameters of ocean and land surface such as sea surface height, ocean wind speed and direction, snow thickness, ice thickness, and soil moisture [7–9].

A concept of heavy rain detection based on polarimetric GNSS-RO signals was proposed by Cardellach et al. in 2010 [10], which provided a new application direction. They aimed to use the double-polarization GNSS receivers placed on Spanish Low Earth Orbiter (LEO) satellite PAZ to receive RO signals across a precipitation area. Then, they did some theoretical research and ground-based field campaign using the polarimetric parameter and polarimetric phase shift, to validate its feasibility [11,12]. Yan et al. [13] had analyzed the sensitivity of cross-polarization discrimination (XPD) of GNSS signals with rain rate by simulation. Up to now, the method of rain rate detection using GNSS signals is still under research.

The goal of this study is to explore the possibility of other polarimetric GNSS propagation parameters for rain monitoring in theory. The polarimetric radio-propagation parameters also contain specific co-polar attenuation, cross-polar attenuation, co-polar phase shift, and specific differential phase shift. Since GNSS signals belong to the L-band [14], rain-induced attenuation is quite weak [15]. Therefore, we mainly investigate the co-polar phase shift and specific differential phase shift of GNSS signals. The occurrence of phase shift is due to the nonspherical shapes of raindrops and the canting of raindrops [16]. Phase shift has been widely utilized in polarimetric weather radar in order to estimate rain rate and analyze the characteristics of different hydrometeors [17,18]. The phase shift in weather radar reflects the backward scattering features of raindrops, while in this study, that of GNSS signals comes from the results of forward scattering.

This paper is organized as follows. Section 2 details the relation models between three polarimetric propagation parameters and rain rate, namely K_{HH}-R, K_{VV}-R, and K_{DP}-R, based on different shapes of raindrops and Gamma raindrop size distribution, respectively. Using simulated raindrop size distribution, the three relation models are simulated and the feasibility of estimating rain rate using these models is analyzed in Section 3; the effects of scattering algorithm, shape of raindrops, frequency, and elevation angle on the three models are also discussed systematically; furthermore, the three relation models are investigated under three different real rain conditions. Section 4 summarizes some meaningful conclusions.

2. Methods

2.1. Shapes of Raindrops

Since it is the main cause of phase shift, considerations regarding the shapes of raindrops are essential for studying phase shift. Their final shapes are affected by hydrostatic, surface tension, and aerodynamic forces [19]. Therefore, they are actually nonspherical. These shapes are often described by axis ratio $r = a/b$, where a and b represent the lengths of semiminor and semimajor axes, respectively. The relation between axis ratio and equivolumetric spherical diameter, also called shape-size relation, was researched by many experts. Pruppacher and Beard [20] developed an empirical linear equation (hereinafter named PB model) by tunnel measurements, which was used in early radar measurements. Based on different experimental data, some nonlinear equations, even fourth-order polynomials, were obtained by other researchers, such as Beard and Chuang (hereinafter named BC model) [21], Brandes et al. (hereinafter named Brandes model) [22], and Thurai et al. (hereinafter named Thurai model) [23]. The expressions of these shape models are listed in Table 1. Here, D_{eq} is the diameter of the equivolumetric spherical drop in mm. Among these shape models, since the BC model introduced aerodynamic pressure to the equilibrium condition, it is more precise and often used in many calculations or regarded as a comparative object [19,24,25]. Therefore, it was selected for our following simulation research.

Table 1. Expressions for different raindrop shape-size relations.

Model	Expressions
PB model:	$r = 1.03 - 0.062D_{eq}\ (1 \le D_{eq} \le 9\ mm)$
BC model:	$r = 1.0048 + 5.7 \times 10^{-4}D_{eq} - 2.628 \times 10^{-2}D_{eq}^2 + 3.682 \times 10^{-3}D_{eq}^3 - 1.677 \times 10^{-4}D_{eq}^4$ $(1 \le D_{eq} \le 7\ mm)$
Brandes model:	$r = 0.9951 + 2.51 \times 10^{-2}D_{eq} - 3.644 \times 10^{-2}D_{eq}^2 + 6.303 \times 10^{-3}D_{eq}^3 - 2.492 \times 10^{-4}D_{eq}^4$ $(1 \le D_{eq} \le 4\ mm)$
Thurai model:	$r = 1.065 - 6.25 \times 10^{-2}D_{eq} - 3.99 \times 10^{-3}D_{eq}^2 + 7.66 \times 10^{-4}D_{eq}^3 - 4.095 \times 10^{-5}D_{eq}^4$ $(1.5 \le D_{eq} \le 9\ mm)$

2.2. Raindrop Size Distribution

Phase shift of GNSS signals is also related to raindrop size distribution. There are many models to express raindrop size distribution, such as Laws-Parsons (LP) [26], Marshall-Palmer (MP), drizzle (JD), thunderstorm (JT) [27], and Gamma distribution [28]. However, according to the analysis data, many naturally occurring raindrop size distributions can be represented by the three-parameter Gamma distribution [28]

$$N(D) = N_0 D^{\mu} \exp(-\Lambda D) \tag{1}$$

where D is diameter of the equivolumetric spherical drop in millimeters; $N(D)dD$ is the number of drops of size D to $D + dD$; N_0 is the intercept parameter in $mm^{-1-\mu} \cdot m^{-3}$; μ is the shape parameter in mm^{-1}; and Λ is the slope parameter in mm^{-1}. The values of these parameters can be obtained from measured raindrop data or radar data. This Gamma distribution is widely accepted and used by radar meteorologists and other researchers to model natural raindrop size distributions [11,29,30]. The rain rate R can be computed from [31]

$$R\left(mm\ h^{-1}\right) = 6 \times 10^{-4}\pi \int N(D)\, V_{\infty}(D)\, D^3 dD \tag{2}$$

with the terminal fall velocity of the drop $V_{\infty}(D)$ in meters per second. There are several empirical formulas to express $V_{\infty}(D)$. A widely used one is given by Gunn and Kinzer [32] as

$$V_{\infty}(D) = 9.65 - 10.3\exp(-0.6D) \tag{3}$$

2.3. Calculation Models of Phase Shift Parameters

These polarimetric propagation parameters, co-polar phase shift (K_{HH}, K_{VV}) and specific differential phase shift (K_{DP}), were considered. They are respectively given by [33]

$$K_{HH} = \frac{180\lambda}{\pi} \int \mathrm{Re}\left(f_{HH}(D,0)\right) N(D) dD \tag{4}$$

$$K_{VV} = \frac{180\lambda}{\pi} \int \mathrm{Re}\left(f_{VV}(D,0)\right) N(D) dD \tag{5}$$

$$K_{DP} = K_{HH} - K_{VV} \tag{6}$$

where λ is the wave length; Re indicates the real part; $N(D)$ is the raindrop size distribution; and f_{HH} and f_{VV} are forward-scattering amplitudes at horizontal and vertical polarization state, respectively. Now, the scattering amplitudes for nonspherical drops can be computed from many algorithms [25]. However, considering the frequencies of GNSS signals (L-band) and the shape-size features of raindrops, the Rayleigh Scattering Approximation and T-matrix are used in this simulation research [16,34,35]. K_{HH}, K_{VV}, and K_{DP} are all in deg·km^{-1} units. In Equations (4)–(6), canting angles of raindrops are assumed to be 0°.

Based on the above equations, the relation models between polarimetric propagation parameters K_{HH}, K_{VV}, K_{DP}, and rain rate R, namely K_{HH}-R, K_{VV}-R, and K_{DP}-R, can be respectively obtained. These relations will be simulated and discussed in the following section to study the feasibility of estimating rain rate.

3. Simulation Analysis and Discussion

3.1. Numerical Simulations Based on Simulated Raindrop Size Distribution

In this simulation, two kinds of scattering algorithms, Rayleigh Scattering Approximation and T-matrix, are selected to compare with each other. In order to use these algorithms, many factors, such as frequency and angle of incident electromagnetic waves, environmental temperature, refractive index of water, shapes of raindrops, as well as raindrop size distribution, are necessary. The L1 (1.57542 GHz) frequency of GPS is used in this paper to serve as an example. For the coordinate system in these algorithms, incident angle can be approximately equal to the elevation angle and is assumed to be 0° here [25,34]. The environmental temperature of 20 °C is used. The refractive index of water is calculated from Ray [36]. The BC model is chosen to express the shapes of raindrops.

Since raindrop size distribution varies largely in different geographical locations and precipitation types, we consider the ranges of three parameters (N_0, μ, Λ) of the Gamma size distribution to simulate natural raindrops size distributions. In considering previous research [19,29,30,37,38], the parameters of Gamma size distribution vary across a wide range and can be defined by

$$300 \leq N_0 \leq 300,000 \tag{7}$$

$$-3 \leq \mu \leq 10 \tag{8}$$

$$3 \leq \Lambda \leq 12 \tag{9}$$

with the additional constraint that $R \leq 100$ mm·h^{-1}.

Figure 1 illustrates the simulated results of K_{HH}-R, K_{VV}-R, and K_{DP}-R relations at the L1 (1575.42 MHz) frequency of GPS signals based on simulated raindrop size distribution using Rayleigh Scattering Approximation (blue asterisk) and T-matrix (blue circles), respectively. It can be easily seen that the three polarimetric propagation parameters generally show upward trends with the increasing rain rate, and even their trends are similar. In these conditions, the value of K_{HH} can be as large as 7 deg·km^{-1}, that of K_{VV} can be more than 6.5 deg·km^{-1}, and the maximum value of K_{DP} is less than 1 deg·km^{-1}. These results are also consistent with previous research by Ajaji [39]. In contrast, the result of the T-matrix exhibited a very consistent correlation with that of the Rayleigh Scattering Approximation. This can be observed from the correlation coefficients for K_{HH}, K_{VV}, and K_{DP} using the two kinds of scattering algorithms, which are all 1.0; and their root mean square errors are 0.0076, 0.0066, and 0.0011, respectively, all of which are rather small. Here, the number of statistical samples is 139,569. Therefore, the effect of scattering algorithms is quite weak, as such the T-matrix is used hereafter.

In Figure 1, the solid red line represents mean values of polarimetric propagation parameters for every constant rain rate. It is noted that for different scattering algorithms, the features of mean values of the three parameters are approximately the same, respectively. The parameters of the Gamma distribution used to derive the red line will be selected in our following simulation.

Figure 1 indicates that the variation of raindrop size distribution can lead to differences in the phase shift, so it is important to get the information of local raindrop size distribution in advance. Certainly, after getting the parameters of Gamma distribution, these polarimetric propagation parameters have the potential to estimate rain rate.

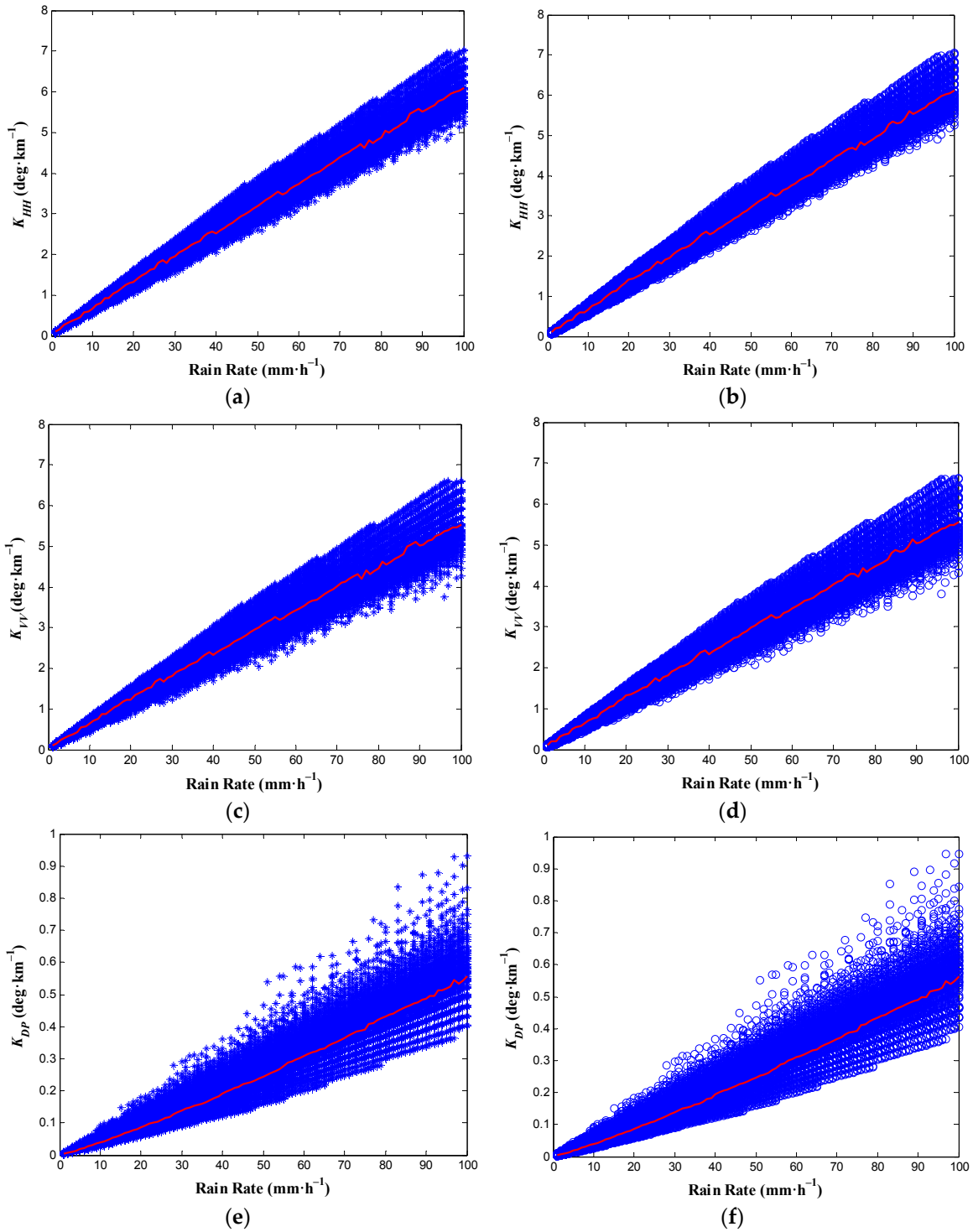

Figure 1. Results of polarimetric propagation parameters vs. rain rate at the L1 (1575.42 MHz) frequency of GPS signals based on simulated raindrop size distribution. (**a**) K_{HH}-R using Rayleigh Scattering Approximation; (**b**) K_{HH}-R using T-matrix; (**c**) K_{VV}-R using Rayleigh Scattering Approximation; (**d**) K_{VV}-R using T-matrix; (**e**) K_{DP}-R using Rayleigh Scattering Approximation; (**f**) K_{DP}-R using T-matrix.

3.2. Sensitivity Analysis of Phase Shift with Respect to Shape of Raindrops

In order to analyze the effect of the shape of raindrops, four different shape models, PB model, BC model, Brandes model, and Thurai model, whose expressions were listed in Table 1, are used.

Other parameters in this simulation have been depicted in Section 3.1. Figure 2 presents the polarimetric propagation parameters against rain rates for various shapes of raindrops at the L1 (1575.42 MHz) frequency of GPS signals. It can be observed that for K_{HH} (Figure 2a) and K_{VV} (Figure 2b) differences in the various shapes of raindrops between the two propagation parameters are not obvious, especially when rain rate is less than 50 mm·h^{-1}. However, when the rain rate becomes higher, K_{HH} is largest in the PB model and smallest at Brandes model, while for K_{VV} it shows the opposite character. Thus, the K_{DP} is largest in the PB model and smallest in the Brandes model. This may be due to the fact that the range of Brandes model's equivolumetric spherical diameter only contains smaller raindrops (shown in Table 1), which induce a less specific differential phase shift.

From Figure 2, the effect of the shape of raindrops is weak when using K_{HH} or K_{VV} to estimate rain rate, while it should be considered when using K_{DP}.

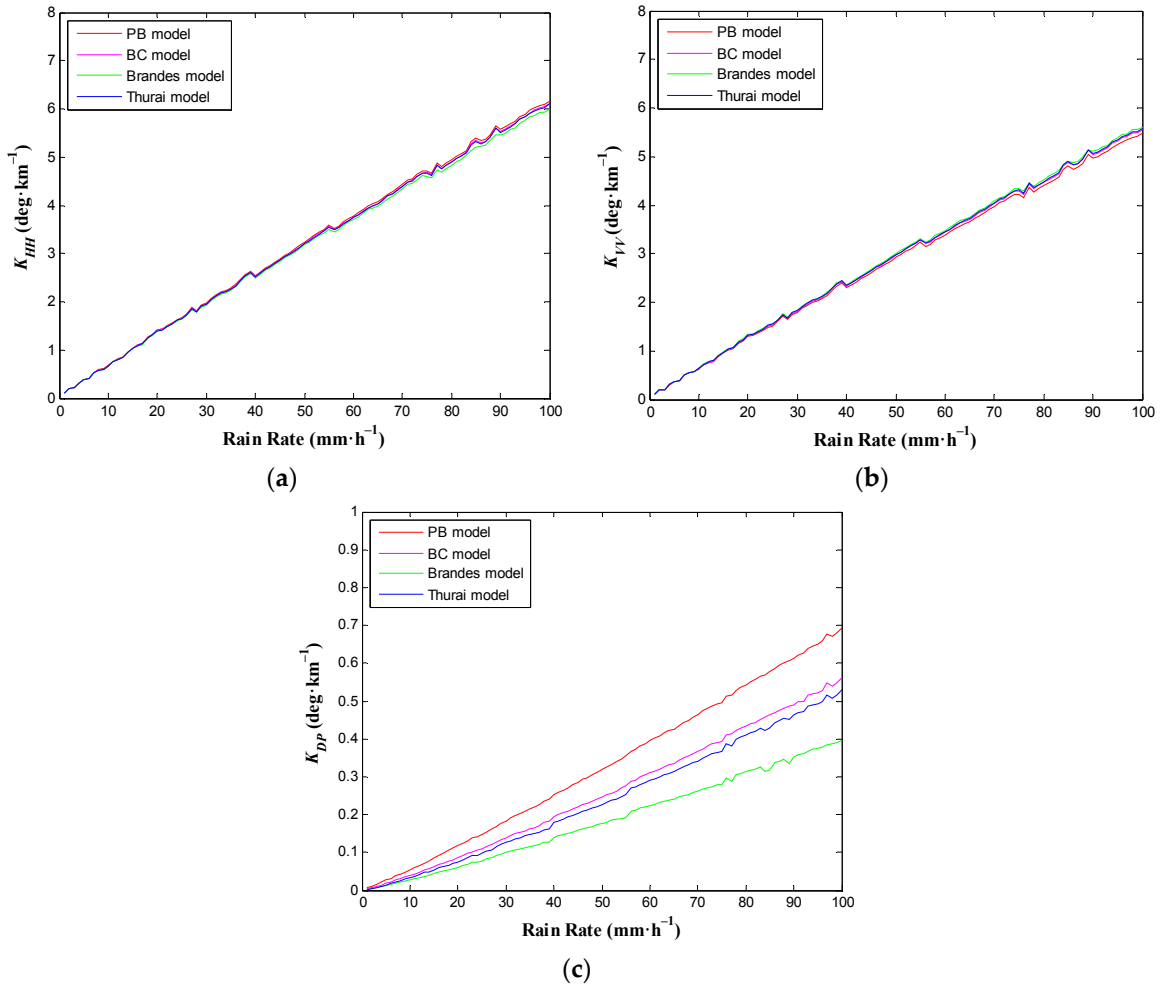

Figure 2. Polarimetric propagation parameters vs. rain rate for various shapes of raindrops at the L1 (1575.42 MHz) frequency of GPS signals. (**a**) K_{HH}-R; (**b**) K_{VV}-R; (**c**) K_{DP}-R.

3.3. Sensitivity Analysis of Phase Shift with Respect to Frequency

Frequency not only has an effect on the refractive index of water, but the free-space wavenumber in calculating forward-scattering amplitudes, finally it also influences the phase shift. To have a view of the effect of different frequencies, GPS L1/L2 (1575.42 MHz/1227.60 MHz) and Beidou B1/B2 (1561.098 MHz/1207.14 MHz) are utilized here. Polarimetric propagation parameters against rain rates for frequencies of GPS and BeiDou signals are shown in Figure 3. It can be seen that polarimetric propagation parameters K_{HH}, K_{VV}, and K_{DP} are all increasing with the growing frequency. Obviously,

the results of L1 frequency are quite close to those of B1 frequency. This is no surprise because their frequencies have little difference. Also, it is similar for the results of L2 and those of B2.

Figure 3 reveals that the effect of frequency is obvious, and in order to get larger K_{HH}, K_{VV}, and K_{DP} when estimating rain rate, higher frequencies L1 and B1 are suggested.

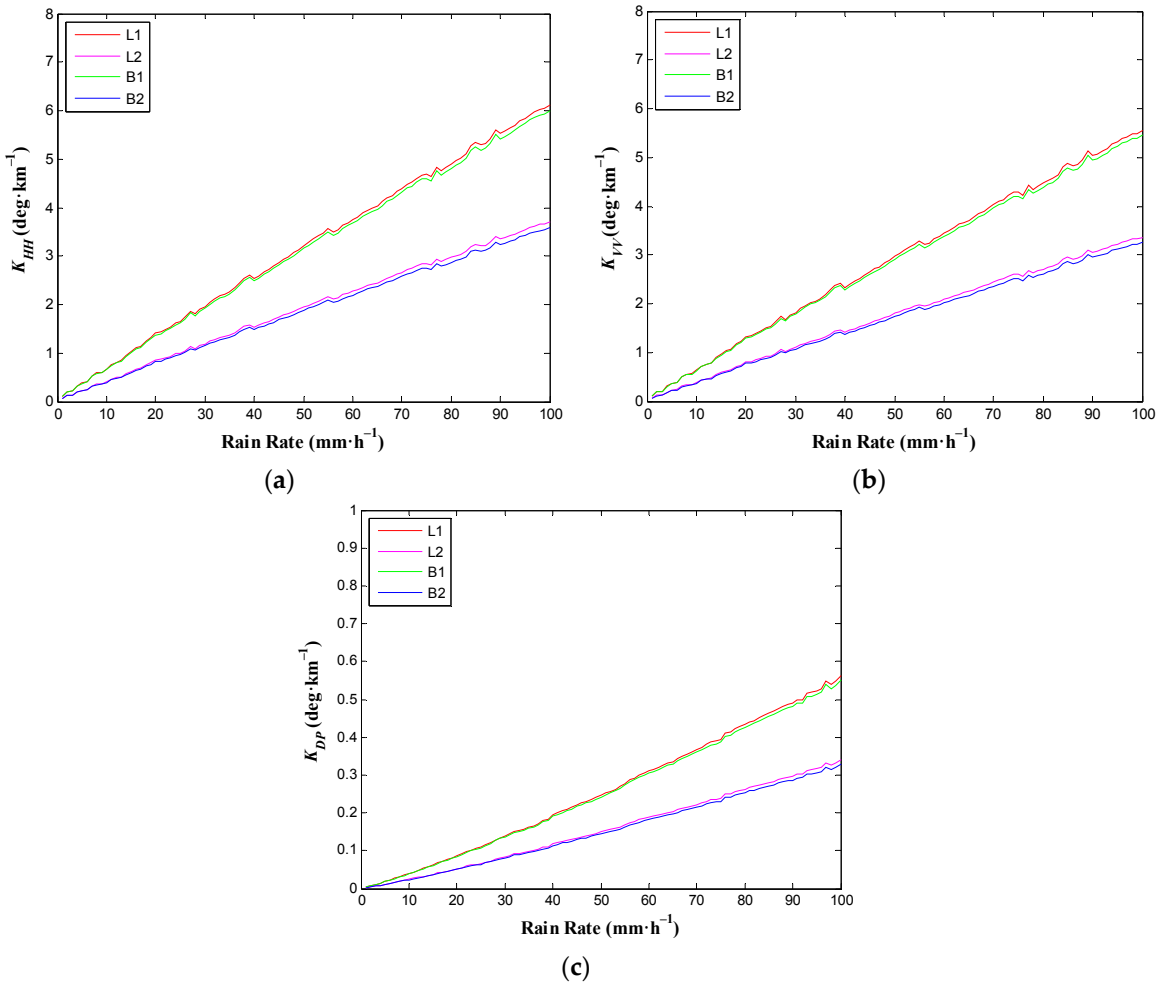

Figure 3. Polarimetric propagation parameters vs. rain rate for frequencies of GPS and BeiDou signals. (**a**) K_{HH}-R; (**b**) K_{VV}-R; (**c**) K_{DP}-R.

3.4. Sensitivity Analysis of Phase Shift with Respect to Elevation Angle

In the T-matrix scattering algorithm, elevation angle is an important input factor. Thus, it is necessary to take the elevation angle of GNSS signals into consideration. The elevation angle is set to 0°, 10°, 20°, 30°, and 40°. Other input factors have been mentioned in Section 3.1. The variations of polarimetric propagation parameters against rain rates for various elevation angles at the L1 (1575.42 MHz) frequency of GPS signals have been calculated and presented in Figure 4. The elevation angle has no effect on K_{HH}, which can be seen in Figure 4a. However, as can be observed from Figure 4b,c, its effect can be noted. K_{VV} can be seen to have increased with the increase of elevation angle while K_{DP} has shown an opposite trend. The maximum difference for K_{DP} using 0° and 40° can reach up to 0.2324 deg·km^{-1}, which is not negligible, and therefore cannot be ignored.

Figure 4 tells us that the elevation angle should be known when using K_{VV} and K_{DP} to get rain rate, while it is not necessary for K_{HH}.

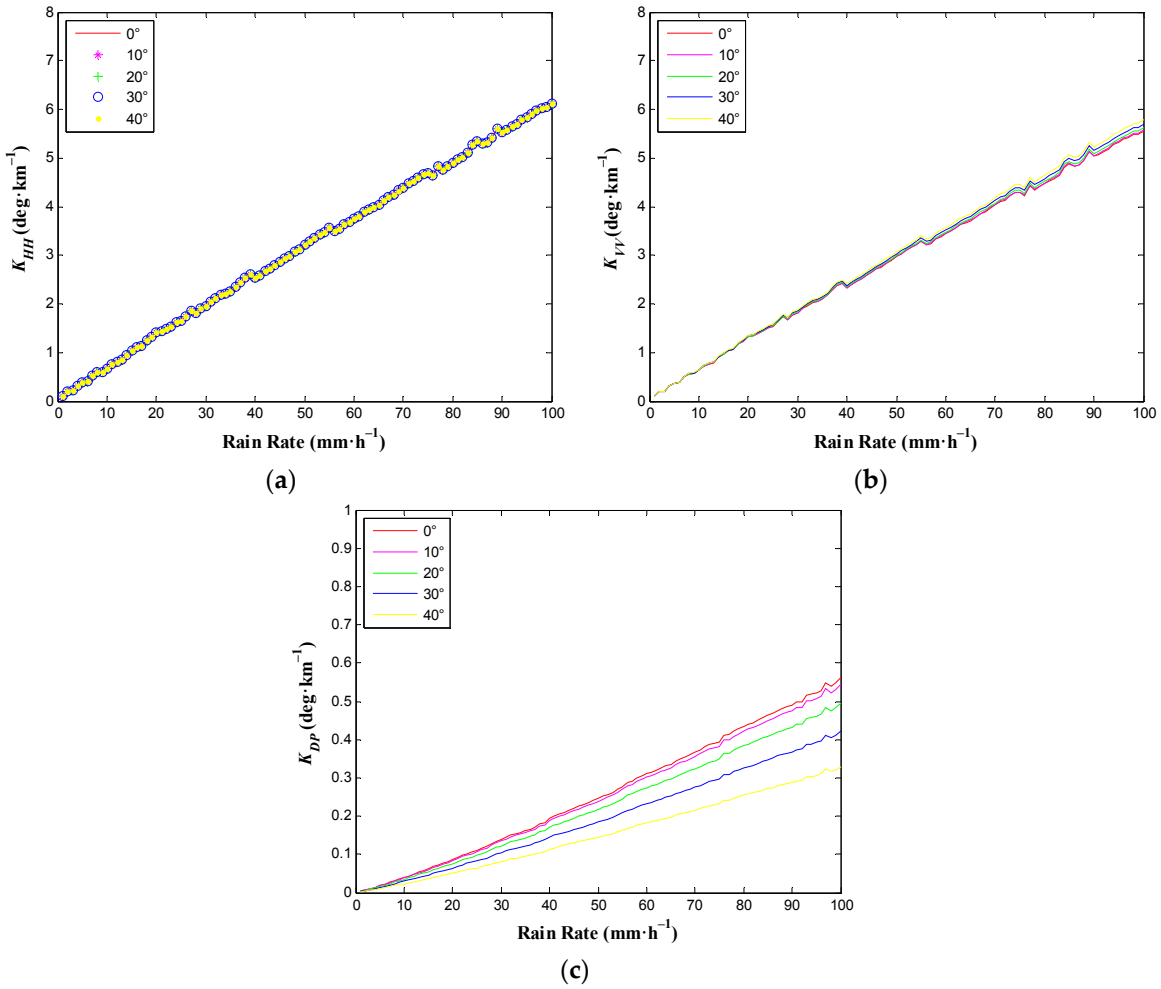

Figure 4. Polarimetric propagation parameters vs. rain rate for various elevation angles at the L1 (1575.42 MHz) frequency of GPS signals. (**a**) K_{HH}-R; (**b**) K_{VV}-R; (**c**) K_{DP}-R.

3.5. Simulation Calculation of Phase Shift under Real Rainfall

In Figure 1 and the above results, it can be seen that the effect of parameters on raindrop size distribution is obvious. In real rainfall, these parameters vary with position and time [28–30,37–40], which is an important factor in the model. In future experiments, we can use local statistical raindrop size distribution data or an empirical model. However, this may cause errors for rain rate estimation. Therefore, if possible, a disdrometer is needed in order to obtain detailed information regarding raindrop size distribution during a rain event. Thus, the errors can be reduced. Here, we take the results of raindrop size distribution obtained from a second-generation one-dimensional (1D) laser-optical disdrometer manufactured by OTT-Germany, which are used to calculate phase shift. The values of three parameters (N_0, μ, Λ) of the Gamma size distribution and the maximum diameters of raindrops during three different rain types, stratiform rain, cumuliform rain, and mixed clouds rain, can be seen in [41]. The results of phase shift under these three rain types are shown in Figure 5.

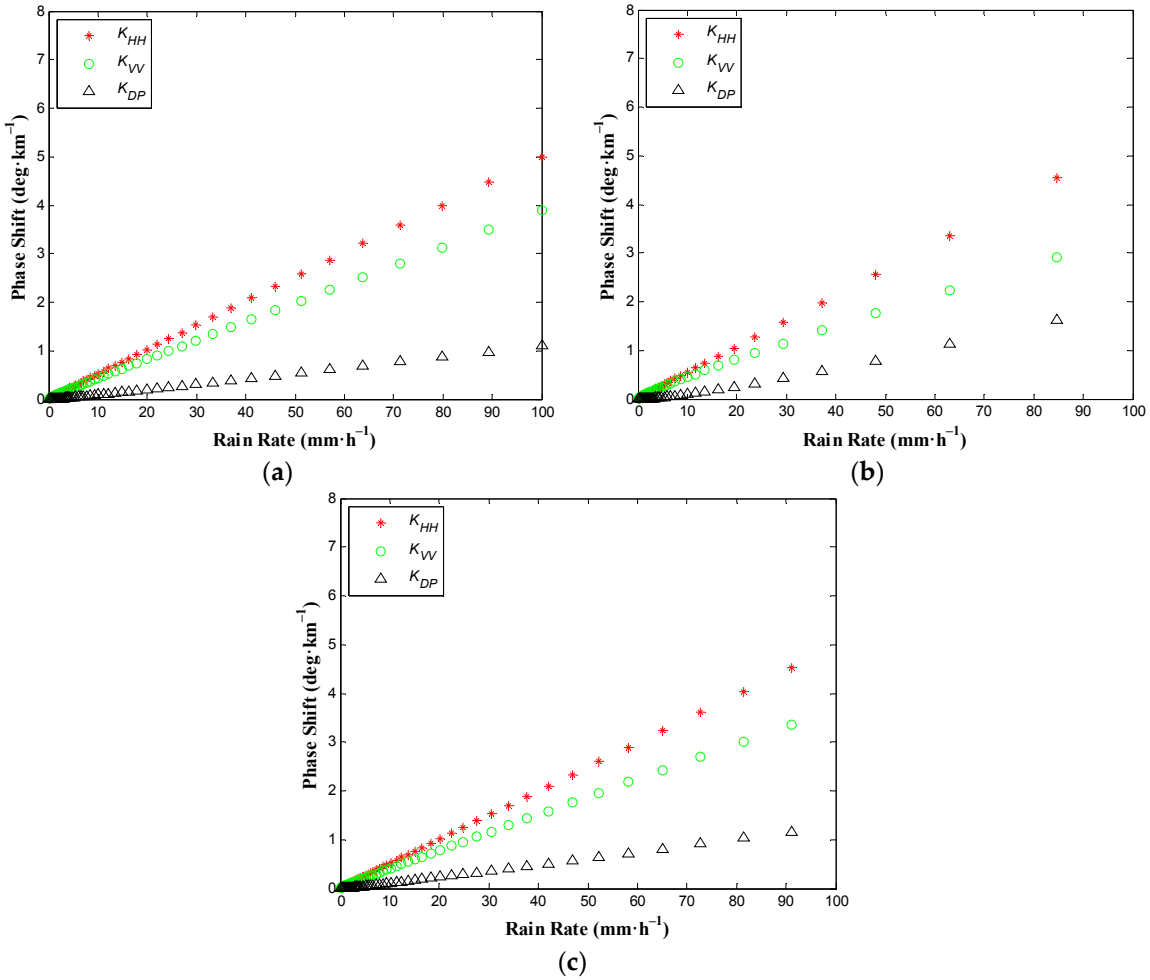

Figure 5. Polarimetric propagation parameters vs. rain rate under three different rain types at the L1 (1575.42 MHz) frequency of GPS signals. (**a**) Stratiform rain; (**b**) cumuliform rain; (**c**) mixed clouds rain.

In Figure 5, since the parameters of raindrop size distribution are variable during the rain process, the phase shift presents different values. The rain rates computed from most of the samples are less than 10 mm·h^{-1}, and the corresponding phase shift is smaller. While the phase shift becomes larger at high rain rates. Also, it can be easily seen that no matter the type of the (real) rain event, the polarimetric propagation parameters K_{HH}, K_{VV}, and K_{DP} all have a notable positive correlation with rain rate. Compared with Figure 1, the values of K_{HH}, K_{VV}, and K_{DP} are all included in the ranges of the results in Figure 1, respectively. Obviously, their values are not the same under different rain types. Especially for K_{VV} and K_{DP}, it seems that K_{VV} is the smallest and K_{DP} is the largest under cumuliform rain. This is caused by the fact that more large-diameter raindrops occur in cumuliform rain and the maximum diameter of raindrops is 7.5–9.5 mm, while in stratiform rain and mixed clouds rain they are 3.25–4.25 mm and 4.25–4.75 mm, respectively [41].

The results calculated from these cases of real rain conditions demonstrate that the polarimetric propagation parameters K_{HH}, K_{VV}, and K_{DP} are still sensitive to rain rate and have the possibility to estimate rain rate using realistic raindrop size distribution. In order to get more accurate phase shift processing, the detailed information of raindrop size distribution is required in experiments.

4. Conclusions

This paper has researched the theoretical feasibility of estimating rain rate based on the polarimetric propagation parameters of GNSS signals. Three theoretical models were set up that

between co-polar phase shift K_{HH}, K_{VV}, specific differential phase shift K_{DP}, and rain rate R, respectively. The models, K_{HH}-R, K_{VV}-R, and K_{DP}-R, were simulated based upon assuming specific ranges of three parameters of Gamma raindrop size distribution and empirical nonlinear shape-size relation of raindrops. The results indicate that they all have the possibility to monitor rain rate. We also compared the results by T-matrix with those by Rayleigh Scattering Approximation, finding that they are very close to each other.

Additionally, some influencing factors, such as the shape of raindrops, frequency, and elevation angle have been considered and their sensitivity has been studied. It was found that the shape of raindrops and frequency of GNSS signals both have effect on the K_{HH}-R, K_{VV}-R, and K_{DP}-R relationships, while the elevation angle only affects the K_{VV}-R and K_{DP}-R relationships. In order to get a larger phase shift, the use of a lower elevation angle and higher frequency L1 or B1 are suggested for future experiments. Moreover, the phase shift has been discussed based on realistic Gamma distribution under three different rain types, and the results also show the feasibility of this method. To reduce errors, the microscopic characteristics of rain, such as the shape of raindrops and raindrop size distribution should be obtained during a precipitation event.

It is quite new to use phase shift to estimate rain rate, which extends the application direction of GNSS signals and provides a new method for the area, real time, and passive measurement of rain rate. Certainly, there are some issues that need to be studied further. However, there is no need to worry about the detectability of phase shift because there are multi-frequency receivers with GPS/Beidou compatibility, which can measure the carrier phase of GPS and Beidou satellites precisely to millimeters [42–44]. However, since an antenna is required to receive horizontal and vertical components of GNSS signals respectively, a dual-polarized antenna should be designed. Then, field campaigns are necessary to examine its validity.

Acknowledgments: This work was supported by the National Natural Science Foundation of China (Grant No. 41375029, Grant No. 41505016, and Grant No. 41306187). The authors are thankful to Estel Cardellach Galí and her team for their sincere help on the measurement of phase shift of GNSS signals. The authors would like to express their thanks to Michael I. Mishchenko and Larry D. Travis for supplying the T-matrix code.

Author Contributions: Wei Yan and Hao An conceived and designed this research; Yingqiang Wang and Weihua Ai made a contribution to the development of the theoretical models; Yunxian Huang and Xianbin Zhao performed the sensitivity analysis; and Hao An wrote the manuscript.

Conflicts of Interest: The authors declare no conflict of interest.

References

1. Jin, S.G.; Cardellach, E.; Xie, F.Q. *GNSS Remote Sensing: Theory, Methods and Applications*; Springer: Berlin, Germany, 2014; pp. 17–240.
2. Bevis, M.; Businger, S.; Herring, T.A.; Rocken, C.; Anthes, R.A.; Ware, R.H. GPS meteorology: Remote sensing of atmospheric water vapor using the Global Positioning System. *J. Geophys. Res.* **1992**, *97*, 15787–15801. [CrossRef]
3. Wang, H.; He, J.; Wei, M.; Zhang, Z. Synthesis analysis of one severe convection precipitation event in Jiangsu using ground-based GPS technology. *Atmosphere* **2015**, *6*, 908–927. [CrossRef]
4. Ware, R.; Rocken, C.; Solheim, F.; Exner, M.; Schreiner, W.; Anthes, R.; Businger, S. GPS sounding of the atmosphere from low Earth orbit: Preliminary results. *Bull. Am. Meteorol. Soc.* **1996**, *77*, 19–40. [CrossRef]
5. Mannucci, A.J.; Wilson, B.D.; Yuan, D.N.; Ho, C.H.; Lindqwister, U.J.; Runge, T.F. A global mapping technique for GPS-derived ionospheric total electron content measurements. *Radio Sci.* **1998**, *33*, 565–582. [CrossRef]
6. Hu, X.; Wu, X.C.; Gong, X.Y.; Xiao, C.Y.; Zhang, X.X.; Fu, Y.; Yang, G.L. An introduction of mountain-based GPS radio occultation experiments in China. *Adv. Space Res.* **2008**, *42*, 1723–1729. [CrossRef]
7. Armatys, M.; Komjathy, A.; Axelrad, P.; Katzberg, S.J. A comparison of GPS and scatterometry sensing of ocean wind speed and direction. In Proceedings of the 2000 IEEE International Geoscience and Remote Sensing Symposium (IGARSS), Honolulu, HI, USA, 24–28 July 2000; pp. 2861–2863.

8. Rius, A.; Nogues-Correig, O.; Ribo, S.; Cardellach, E.; Oliveras, S.; Valencia, E.; Park, H.; Tarongi, J.M.; Camps, A.; van der Marel, H.; et al. Altimetry with GNSS-R interferometry: First proof of concept experiment. *GPS Solut.* **2012**, *16*, 231–241. [CrossRef]
9. Najibi, N.; Jin, S. Physical reflectivity and polarization characteristics for snow and ice-covered surfaces interacting with GPS signals. *Remote Sens.* **2013**, *5*, 4006–4030. [CrossRef]
10. Cardellach, E.; Rius, A.; Cerezo, F. Polarimetric GNSS Radio-Occultations for heavy rain detection. In Proceedings of the 2010 IEEE International Geoscience and Remote Sensing Symposium (IGARSS), Honolulu, HI, USA, 25–30 July 2010; pp. 3841–3844.
11. Cardellach, E.; Tomás, S.; Oliveras, S.; Padullés, R.; Rius, A.; de la Torre-Juarez, M.; Joseph Turk, F.; Ao, C.O.; Kursinski, E.R.; Schreiner, B.; et al. Sensitivity of PAZ LEO polarimetric GNSS radio-occultation experiment to precipitation events. *IEEE Trans. Geosci. Remote Sens.* **2015**, *53*, 190–206. [CrossRef]
12. Padullés, R.; Cardellach, E.; de la Torre Juárez, M.; Tomás, S.; Turk, F.J.; Oliveras, S.; Rius, A. Atmospheric polarimetric effects on GNSS radio occultations: The ROHP-PAZ field campaign. *Atmos. Chem. Phys.* **2016**, *16*, 635–649. [CrossRef]
13. Yan, W.; An, H.; Fu, Y.; Han, Y.; Wang, X.; Ai, W. A method for estimating rain rate from polarimetric GNSS measurements: Preliminary analysis. *Atmos. Res.* **2014**, *149*, 70–76. [CrossRef]
14. Thombre, S.; Hurskainen, H.; Nurmi, J. Wideband, high gain, high linearity, low noise amplifier for GNSS frequencies with compensation for low frequency instability. In Proceedings of the 2010 5th Advanced Satellite Multimedia Systems Conference and the 11th Signal Processing for Space Communications Workshop, Cagliari, Italy, 13–15 September 2010; pp. 349–354.
15. International Telecommunications Union (ITU). *Recommendation ITU-R P.838-3 Specific Attenuation Model for Rain for Use in Prediction Methods*; ITU: Geneva, Switzerland, 2003.
16. Oguchi, T. Electromagnetic Wave Propagation and Scattering in Rain and Other Hydrometeors. *Proc. IEEE* **1983**, *71*, 1029–1079. [CrossRef]
17. Goddard, J.W.; Cherry, S.M. The ability of dual-polarization radar (copolar linear) to predict rainfall rate and microwave attenuation. *Radio Sci.* **1984**, *19*, 201–208. [CrossRef]
18. Notaroš, B.M.; Bringi, V.N.; Kleinkort, C.; Kennedy, P.; Huang, G.-J.; Thurai, M.; Newman, A.J.; Bang, W.; Lee, G. Accurate characterization of winter precipitation using multi-angle snowflake camera, visual hull, advanced scattering methods and polarimetric radar. *Atmosphere* **2016**, *7*, 81. [CrossRef]
19. Gorgucci, E.; Baldini, L. An examination of the validity of the mean raindrop-shape model for dual-polarization radar rainfall retrievals. *IEEE Trans. Geosci. Remote Sens.* **2009**, *47*, 2752–2761. [CrossRef]
20. Pruppacher, H.R.; Beard, K.V. A wind tunnel investigation of the internal circulation and shape of water drops falling at terminal velocity in air. *Q. J. R. Meteorol. Soc.* **1970**, *96*, 247–256. [CrossRef]
21. Beard, K.V.; Chuang, C. A new model for the equilibrium shape of raindrops. *J. Atmos. Sci.* **1987**, *44*, 1509–1524. [CrossRef]
22. Brandes, E.A.; Zhang, G.; Vivekanandan, J. Experiments in rainfall estimation with a polarimetric radar in a subtropical environment. *J. Appl. Meteorol.* **2002**, *41*, 674–685. [CrossRef]
23. Thurai, M.; Huang, G.J.; Bringi, V.N.; Randeu, W.L.; Schönhuber, M. Drop shapes, model comparisons, and calculations of polarimetric radar parameters in rain. *J. Atmos. Ocean. Technol.* **2007**, *24*, 1019–1032. [CrossRef]
24. Bahrami, M.; Mohassel, J.R.; Taheri, M.M. An exact solution of coherent wave propagation in rain medium with realistic raindrop shapes. *Prog. Electromagn. Res.* **2008**, *79*, 107–118. [CrossRef]
25. An, H.; Yan, W.; Huang, Y.; Ai, W.; Wang, Y.; Zhao, X.; Huang, X. GNSS Measurement of Rain Rate by Polarimetric Phase Shift: Theoretical Analysis. *Atmosphere* **2016**, *7*, 101. [CrossRef]
26. Laws, J.O.; Parsons, D.A. The relation of raindrop-size to intensity. *Trans. Am. Geophys. Union* **1943**, *24*, 452–460. [CrossRef]
27. Olsen, R.L.; Rogers, D.V.; Hodge, D.B. The aR^b relation in the calculation of rain attenuation. *IEEE Trans. Antennas Propag.* **1978**, *26*, 318–329. [CrossRef]
28. Ulbrich, C.W. Natural variations in the analytical form of the raindrop-size distribution. *J. Clim. Appl. Meteorol.* **1983**, *22*, 1764–1775. [CrossRef]
29. Chandrasekar, V.; Bringi, V.N. Simulation of radar reflectivity and surface measurements of rainfall. *J. Atmos. Ocean. Technol.* **1987**, *4*, 464–478. [CrossRef]

30. Bringi, V.N.; Chandrasekar, V.; Hubbert, J.; Gorgucci, E.; Randeu, W.L.; Schoenhuber, M. Raindrop size distribution in different climatic regimes from disdrometer and dual-polarized radar analysis. *J. Atmos. Sci.* **2003**, *60*, 354–365. [CrossRef]
31. Atlas, D.; Ulbrich, C.W. Path- and area-integrated rainfall measurement by microwave attenuation in the 13 cm band. *J. Appl. Meteorol.* **1977**, *16*, 1322–1331. [CrossRef]
32. Gunn, R.; Kinzer, G.D. The terminal velocity of fall for water droplets in stagnant air. *J. Meteorol.* **1949**, *6*, 243–248. [CrossRef]
33. Montopoli, M.; Botta, G.; Marzano, F.S. Modeling polarimetric microwave propagation parameters from globally distributed raindrop size distribution measurements. In Proceedings of the 3rd European Conference on Antennas and Propagation (EuCAP 2009), Berlin, Germany, 23–27 March 2009.
34. Mishchenko, M.I.; Travis, L. Capabilities and limitations of a current FORTRAN implementation of the T-matrix method for randomly oriented, rotationally symmetric scatterers. *J. Quant. Spectrosc. Radiat. Transf.* **1998**, *60*, 309–324. [CrossRef]
35. Duffo, N.; Vall llossera, M.; Camps, A.; Corbella, I.; Torres, F. Polarimetric emission of rain events: Simulation and experimental results at X-Band. *Remote Sens.* **2009**, *1*, 107–121. [CrossRef]
36. Ray, P.S. Broadband complex refractive indices of ice and water. *Appl. Opt.* **1972**, *11*, 1836–1844. [CrossRef] [PubMed]
37. Bringi, V.N.; Huang, G.J.; Chandrasekar, V.; Gorgucci, E. A methodology for estimating the parameters of a gamma raindrop size distribution model from polarimetric radar data: Application to a squall-line event from the TRMM/Brazil campaign. *J. Atmos. Ocean. Technol.* **2002**, *19*, 633–645. [CrossRef]
38. Gorgucci, E.; Scarchilli, G.; Chandrasekar, V. Specific differential phase estimation in the presence of nonuniform rainfall medium along the path. *J. Atmos. Ocean. Technol.* **1999**, *16*, 1690–1697. [CrossRef]
39. Ajaji, G.O. Characteristics of rain induced attenuation and phase shift at cm and mm waves using a tropical raindrop size distribution model. *Int. J. Infrared Millim. Waves* **1985**, *6*, 771–806. [CrossRef]
40. Xie, Y.; Chen, Z.; Dai, J.; Hu, P. Analysis on raindrop spectrum in four types of precipitation in Shanghai. *J. Meteorol. Sci.* **2015**, *35*, 353–361.
41. Xiong, F.; Zhou, Y. Study of Moment Methods in Estimating Three Parameters of Gamma Raindrop Size Distribution. *Meteorology* **2016**, *42*, 777–789.
42. Hajj, G.A.; Kursinski, E.R.; Romans, L.J.; Bertiger, W.I.; Leroy, S.S. A technical description of atmospheric sounding by GPS occultation. *J. Atmos. Sol. Terr. Phys.* **2002**, *64*, 451–469. [CrossRef]
43. García, J.G.; Mercader, P.I.; Muravchik, C.H. Use of GPS carrier phase double differences. *Latin Am. Appl. Res.* **2005**, *35*, 115–120.
44. Bai, W.H.; Sun, Y.Q.; Du, Q.F.; Yang, G.L.; Yang, Z.D.; Zhang, P.; Bi, Y.M.; Wang, X.Y.; Cheng, C.; Han, Y. An introduction to the FY3 GNOS instrument and mountain-top tests. *Atmos. Meas. Tech.* **2014**, *7*, 1817–1823. [CrossRef]